Available online at www.sciencedirect.com

SciVerse ScienceDirect

journal homepage: www.elsevier.com/locate/he

A direct flame solid oxide fuel cell for potential combined heat and power generation

Xingbao Zhu [a,b,*], Bo Wei [a], Zhe Lü [a], Lei Yang [b], Xiqiang Huang [a], Yaohui Zhang [a], Meilin Liu [b]

[a] Center for Condensed Matter Science and Technology, Department of Physics, Harbin Institute of Technology, Harbin, Heilongjiang 150080, PR China

[b] School of Materials Science and Engineering, Georgia Institute of Technology, Atlanta, GA 30332-0245, USA

ARTICLE INFO

Article history:
Received 28 December 2011
Received in revised form
21 February 2012
Accepted 26 February 2012
Available online 27 March 2012

Keywords:
Direct flame SOFC
Perovskite anode
Heat and power
Infiltration LSCM
Ni catalyst

ABSTRACT

A sealant-free solid oxide fuel cell (SOFC) micro-stack was successfully operated inside a liquefied petroleum gas (LPG) flame during cooking. This micro-stack consisted of 4 single cells with infiltrated $La_{0.75}Sr_{0.25}Cr_{0.5}Mn_{0.5}O_{3-\delta}$ (LSCM) based composite anodes, achieving an open circuit voltage of 0.92 V and a peak power density of 348 mW cm^{-2}. This performance is significantly better than that of stack with its cathode operation outside flame. The results confirmed that the perovskite oxide anode showed good properties of carbon-free, redox-stability, quick-start (less than 1 min) and successful operation under a wide range of oxygen partial pressure. For comparison, the conventional Ni/yttria-stabilized zirconia (Ni/YSZ) anode was prepared and tested under the same conditions, showing an open circuit voltage of 0.915 V and a peak power density of 366 mW cm^{-2}, but obvious carbon deposition, poor stability and slow/difficult-start. The direct flame SOFC (DFFC) with a new configuration and design has a potential for combined heat and power generation for many applications.

1. Introduction

Combined heat and power (CHP) or co-generation is an ideal application for fuel cells when operating under high temperatures [1–3]. Fuel cells are quiet, compact power generators without moving parts, with hydrogen and oxygen to make electricity and; at the same time, can provide heat for a wide range of applications [1]. In general, fuel cells show high electrical efficiencies under varying load and; thus, result in low emissions. Among five major fuel cell technologies, phosphoric acid fuel cells (PAFCs) are the most mature in commercial production; and recently proton exchange membrane fuel cells (PEMFCs) have also been made some efforts on its CHP application [1,3,4]. With all solid-state ceramic construction, solid oxide fuel cells (SOFCs) share some important characteristics, such as stability, reliability and enhanced efficiency [5,6]. In addition, a variety of hydrocarbons can be used, as fuels for SOFCs, like gasoline, methanol and natural gas. As another asset, the high operating temperature makes internal reforming possible and

* *Corresponding author*. Center for Condensed Matter Science and Technology, Department of Physics, Harbin Institute of Technology, Harbin, Heilongjiang 150080, PR China. Tel./fax: +86 451 86418420.
E-mail address: zhuxingbao008@163.com (X. Zhu).

0360-3199/$ – see front matter Copyright © 2012, Hydrogen Energy Publications, LLC. Published by Elsevier Ltd. All rights reserved.
doi:10.1016/j.ijhydene.2012.02.161

removes the need for a precious metal catalyst, and also produces high grade waste heat suited well to CHP applications [7,8].

Regrettably, the system research about the CHP applications of SOFCs is limited due to their disadvantages when the conventional test configurations were used with CHP technology [9–11]. A conventional SOFC has a dual-chamber configuration: the anode is exposed to a fuel whereas the cathode is exposed to an oxidant (usually air) with the two electrode compartments separated by a hermetic seal [12–14]. Although high-performance of SOFC can be achieved with this configuration, it may not be ideally suited for certain applications, especially small-scale portable applications subject to temperature change or other variations that may lead to problems due to seal failures [15]. These challenges can be alleviated by operating SOFCs in a sealant-free single-chamber configuration, in which both anode and cathode are exposed to the same fuel-oxidant mixture. The successful operation of such a single-chamber SOFC relies on the selective catalytic activities of its anode and cathode towards the fuel and oxidant, respectively [16–18]. To date, unfortunately, the selective activity of both anode and cathode materials studied for this application are still not satisfactory for practical application. In addition, the mixture of fuel and oxidant poses serious safety concerns because it is vulnerable to explosion [19]. Recently, another type of sealant-free SOFC, direct flame fuel cells (DFFCs) was proposed by Michio et al. [20,21]. In this configuration, the anode is directly exposed to a fuel-rich flame while the cathode is open to ambient air. The flame serves as a fuel-flexible reformer through partial oxidation while supplying the heat for thermally sustaining the electrode reactions. When properly designed, a complex thermal management system is no longer needed; this feature is especially important to portable applications [22,23]. Currently, the development of DFFC is still in its infancy and many parameters are yet to be explored to obtain reasonable performance [24,25]. For example, the output voltages of a DFFC depend critically on the location of the cell relative to the flame [26]. On one hand, the cell must be placed away from the flame in order to maintain high oxygen partial pressure around the cathode. On the other hand, however, the temperature drops off quickly away from the flame so that the cell temperature is too low away from flame, leading to low performance and poor stability [26]. If the whole cell is placed inside a flame, the cell temperature and stability can be improved but proper gas manifold should be provided to maintain reasonably high partial pressure of oxygen on the cathodes.

Here we report our findings on fabrication and operation of a 4-cell micro-stack inside a liquefied petroleum gas (LPG) flame while the waste heat was used for heating water. The fuel cell stack was cycled thermally for 5 times and run in the LPG flame for more than 30 h (cumulative) without observable degradation in performance. Moreover, this sealant-free configuration can effectively avoid disadvantages of conventional configurations, such as seal fails of dual-chamber SOFCs and low selective catalytic activities of electrodes in single-chamber SOFCs. Additionally, the operating stabilities of DFFCs were also improved significantly as the new configuration became available. Thus, this configuration is more suitable for portable application.

2. Experimental

2.1. SOFC fabrication

The typical SOFCs were all based on the configuration of infiltrated anode/membrane electrolyte/slurry cathode, and the process flow of preparation was displayed in Fig. 1. The anode for the single cell was prepared by infiltrating an aqueous solution onto a scaffold of yttria-stabilized zirconia (YSZ) with a porosity of ~70%. The YSZ electrolyte membrane was prepared using a spin coating technique, followed by firing at 1400 °C for 4 h. The cathode of $La_{0.8}Sr_{0.2}MnO_{3-\delta}$ (LSM) with a rectangular shape and effective geometric surface area of about 0.16 cm^2 was prepared by brush painting of LSM slurry on YSZ followed by firing at 1100 °C for 2 h. The anode preparation was conducted by infiltrating a mixed nitrate solution containing La^{3+}, Sr^{2+}, Cr^{3+}, Mn^{2+}, Ni^{2+} and urea with a molar ratio of 75:25:50:50:40:400. The infiltrated coatings were co-fired with LSM slurry at 1100 °C for 2 h to form the anticipated phases of anode and cathode.

2.2. Experimental setup

The anodes of four single cells were attached onto a stainless-steel mesh (120 mesh) using Ag paste, and the mesh was then fixed to a hollow stainless-steel block (30 × 15 × 10 mm^3) with the four cathodes directly facing four holes (9.7 mm in diameter) on the both sides of the block. Not that there was no sealant between the cells and the block, as shown in Fig. 2. Two stainless-steel tubes (33 mm in length and 3 mm inner diameter) were welded on both ends of the block, which is used as the support of block and guide-channel for air flow. Ag paste was used as current collector and Ag wire could be used as the lead wire to cathodes since it will be no exposure to flame directly with the protection of stainless-steel tube. As for anodes, however, Ag paste was still used as current collector and stainless-steel meshes should be used as lead wires since it can be directly exposed to flame.

2.3. Cell characterization

A gas cooking top (usually used for cooking in kitchen) was used to provide the heat and fuel (with flame) for the operation of 4-cell micro-stack that was placed in LPG flame under an aluminum saucepan, as schematically shown in Fig. 2. Four K-type thermocouples were mounted on the anode side to monitor cells temperatures. The cells voltages and currents were recorded using an electrochemical interface (Solartron SI 1287). The morphology and carbon deposition of anode were examined using a scanning electron microscope (SEM, Hitachi S-4800).

3. Results and discussion

3.1. Structural characterization

After infiltration of the mixed nitrate solution for many times, the YSZ matrix was sintered at 1100 °C for 2 h. X-ray

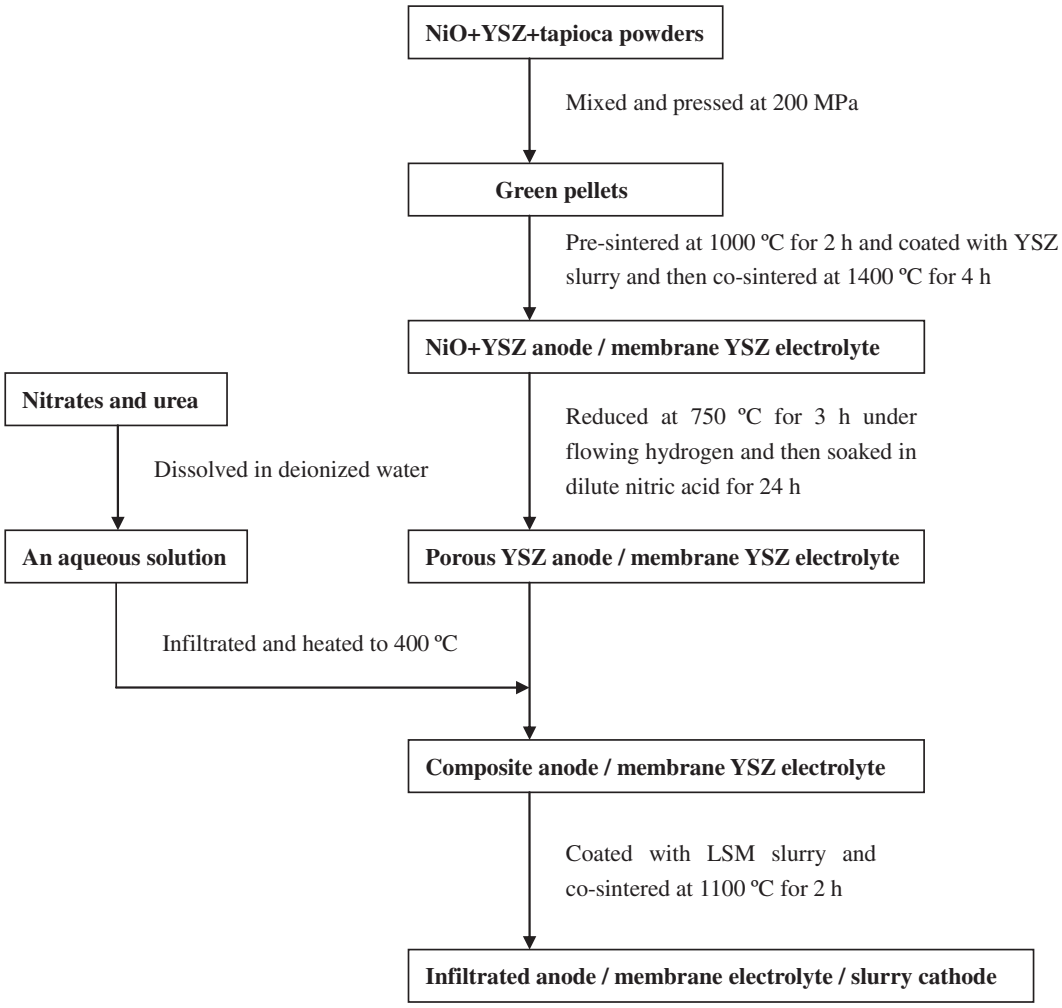

Fig. 1 – A flow chart for preparation of the typical single SOFCs.

diffraction (XRD) was then used to confirm the anode components. A perovskite phase was obtained, which should include $(La_{0.75}Sr_{0.25})(Cr,Mn)O_{3-\delta}$, $(La_{0.75}Sr_{0.25})(Cr,Ni)O_{3-\delta}$ and $(La_{0.75}Sr_{0.25})(Cr,Mn,Ni)O_{3-\delta}$, since Ni can be doped on the Cr-site due to a similar ionic radius [26,27]. Among them, $La_{0.75}Sr_{0.25}Cr_{0.5}Mn_{0.5}O_{3-\delta}$ (LSCM) should account for the vast majority, because La^{3+}, Sr^{2+}, Cr^{3+} and Mn^{2+} were added at a molar ratio of 75:25:50:50, corresponding to the formal of $La_{0.75}Sr_{0.25}Cr_{0.5}Mn_{0.5}O_{3-\delta}$. And, the main peaks of the NiO (JCPDS card no. 44-1159) can be detected obviously (Fig. 3), without peaks of MnO_x and CrO_x. This implies that the solubility of Ni is weaker compared to Mn and Cr, so nickel oxide particles separate out during the heating process for perovskite phase formation. This conclusion has also been confirmed by the study of T. Jardiel, the exsolution of Ni could be obtained from the LSCM nickel-substituted compounds, and which was detected by a transmission electron microscope (TEM) [28]. In addition, the conductivities of these substituted phases are slightly higher than those corresponding to the undoped materials. The total conductivity for the doped material seems to be mainly p-type and the substitution with Ni essentially affects the Mn^{3+}/Mn^{4+} valence ratio, demonstrating that the amount of Ni was not enough to form the electronic conductivity network [28]. It can also be seen from the XRD results that most of the Ni element in this infiltrated anode is still in the form of NiO as expected, which is helpful for anode catalytic activity [29].

3.2. *Effect of air flow on cell performance*

As discussed earlier, the single cells were directly contacted with the stainless-steel block without using any sealants between the cell and the stainless-steel block in order to minimize or eliminate the thermal stress between cell components. Thus, some mixing between the fuel stream (from the anode side) and air (from the cathode side) is inevitable, resulting in low open circuit voltage (OCV). That is because the OCV of SOFC was mainly determined by the difference of partial pressures between anode and cathode, according to Nernst equation [30,31]. To minimize this gas mixing, the flow rate of air onto the cathode side was adjusted. Fig. 4 shows the change of OCV values of the 4-cell stack with the air flow rate to cathode side. Clearly, as the air flow rate was increased to a threshold value of ~150 standard cubic centimeter per minute (sccm), the OCV approached ~0.9 V. It appears that, below this threshold

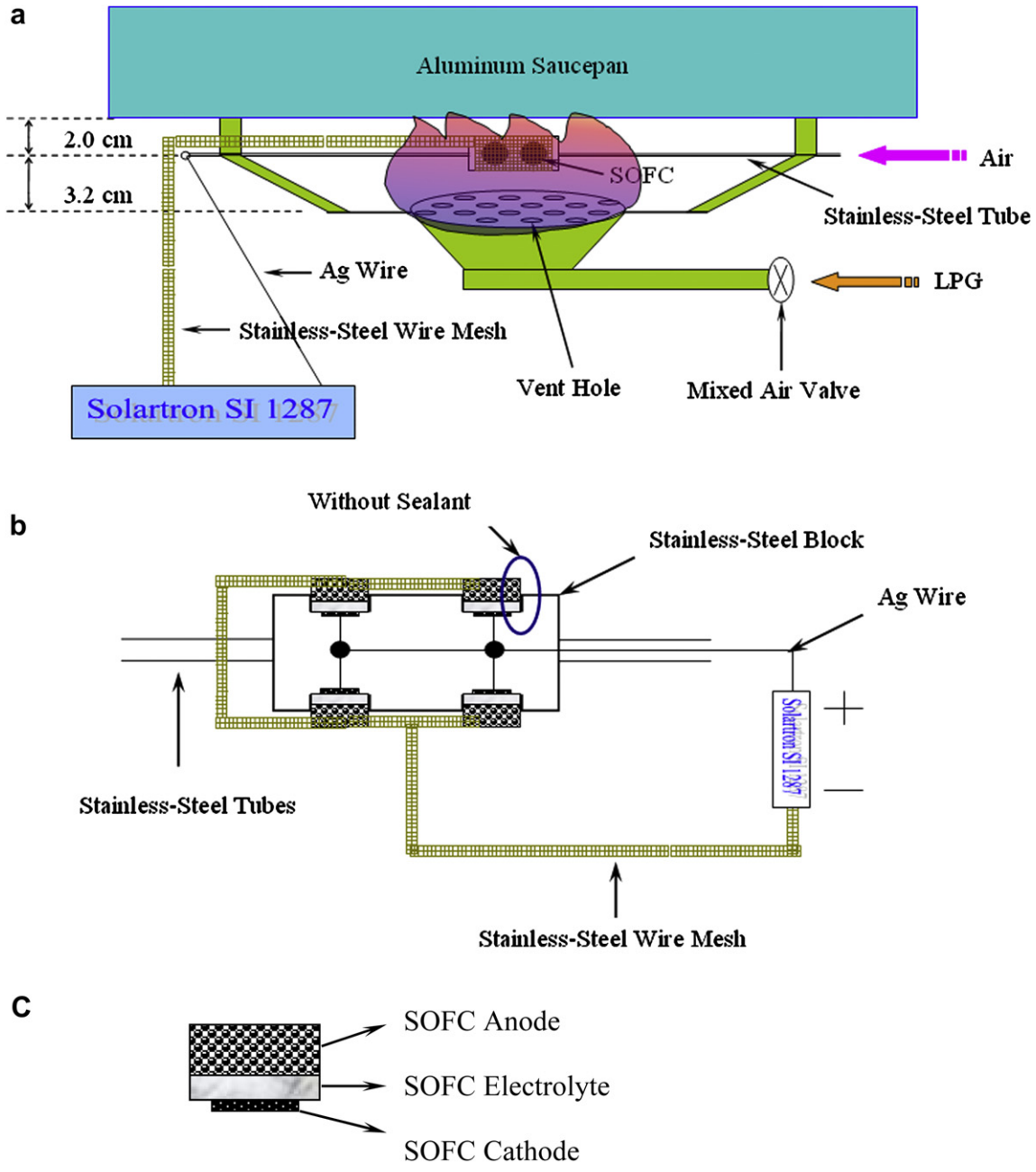

Fig. 2 – Experimental setup: (a) schematic arrangement for testing of a 4-cell stack in an open flame of LPG used for a typical cooking top; (b) setup with 4-cell stack and (c) schematic diagram of the typical SOFC configuration.

value the air flow can not effectively count the diffusion of fuel to cathode side, leading to a depletion of oxygen near the cathode and hence low OCV. When the air flow rate is greater than this threshold value, the effect on OCV is relatively small. There appears to be a large window in air flow rate within which the OCV is relatively insensitive to air flow rate. This can be explained as follows. As the air flow rate was increased from 150 to 250 sccm, the partial pressure of oxygen near the cathode surface was increased slightly, leading to a small increase in OCV (reaching >0.9 V). Further increase in air flow rate led to more air spreading from the cathode side to the anode side, which was burned in the flame, releasing heat.

The corresponding peak power densities of the 4-cell stack under different air flow rates were given in Fig. 5. The changing trend of the 4-cell stack performance with air flow rate is similar to that of OCV. The threshold value of air flow rate for peak power density was also 150 sccm. It can be seen that the values of OCV and peak power density increased gradually when air flow rate increased from 150 sccm to 250 sccm. The gradually increase should be attributed to two factors: one is the increasing partial pressure of oxygen around cathode; the other is the increasing temperature of cells themselves. When increasing air flow rate from 150 sccm to 250 sccm, the cell temperature was found to increase from 821 °C to 837 °C.

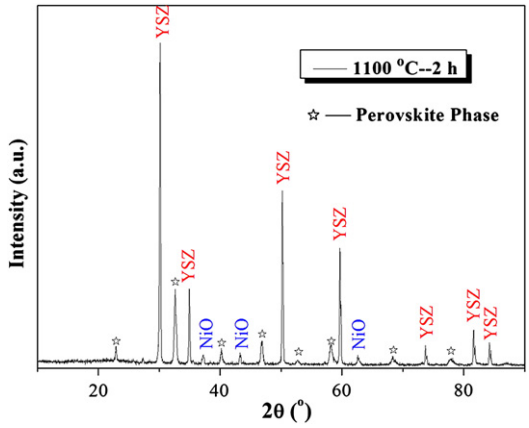

Fig. 3 – X-ray diffraction scans from a typical infiltrated anode used in this study. The peaks corresponding to YSZ and NiO were marked.

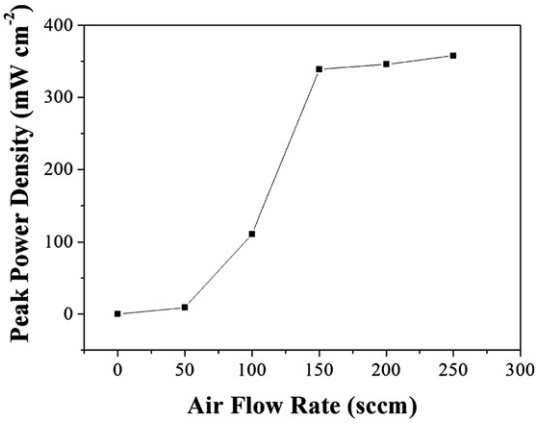

Fig. 5 – Peak power densities of a 4-cell stack with infiltrated anode measured as a function of the flow rate of air onto the cathode side.

3.3. *Start-up time for direct flame SOFC*

When ignited, the SOFC will be exposed to flame and NiO in anode will be reduced to Ni catalyst. The start-up time for DFFC is the same as the time it takes to reduce the cell anode to the desired phases and thus reach stable performance. The OCV values of the 4-cell stack with infiltrated anode were recorded in Fig. 6, as a function of time after exposure of the anode to LPG flame. When the air flow rate to cathode was kept at 200 sccm (and the largest flow of LPG and middle mixed air to anode), it took less than 1 min for the cell OCV to increase from 0 V to 0.96 V, implying that the infiltrated anode is reduced/activated quickly due to a small amount of NiO inside anode. This also suggests that the start-up time for this direct-flame configuration is much shorter than those for conventional dual- and single-chamber configurations that must need a continuous increase of temperature for external heating device [18]. In this study, the typical anodes are all based on LSCM perovskite oxides that are no need to be reduced. So, the infiltrated anode do not need an additional reduction step before test, which is more convenient than the conventional NiO based anodes that must be reduced before single-chamber or direct-flame test [17].

For comparison, a similar 4-cell stack with conventional Ni/yttria-stabilized zirconia (Ni/YSZ) anode was tested under the same conditions. The cells anodes of Ni/YSZ were prepared as stated before [32], and the experimental setup was the same as mentioned above. Fig. 7 compares the reduction/activation times for the two kinds of anodes, infiltrated anode and Ni/YSZ anode, under direct LPG flame conditions. Experiments were conducted under three conditions corresponding to three different flow rates of mixed air to anode. It can be seen that the time required for the reduction/activation of perovskite based anode was almost the same, 0.6, 0.6 and 0.8 min, when the flow rates of LPG and mixed air to anode were adjusted to (Maximum, Minimum), (Maximum, Middle) and (Maximum, Maximum). It indicates that the perovskite based anode is easy to be reduced/activated, and the required time is insensitive to oxygen content.

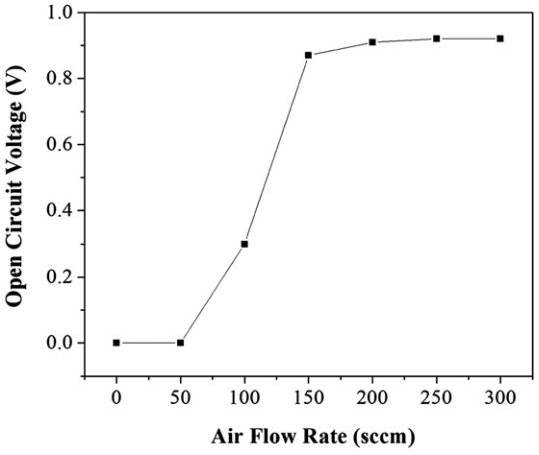

Fig. 4 – Open circuit voltages (OCV) of a 4-cell stack with infiltrated anode measured as a function of the flow rate of air onto the cathode side.

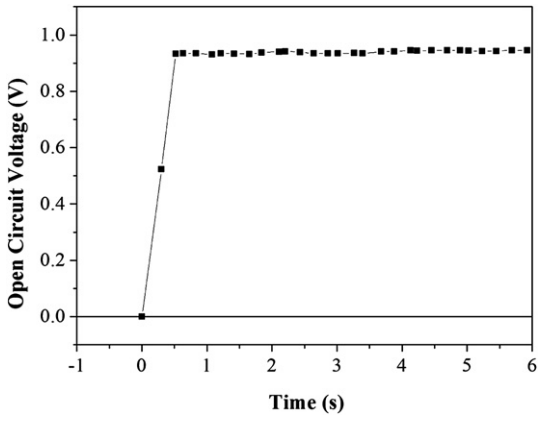

Fig. 6 – Open circuit voltages (OCV) of a 4-cell stack with infiltrated anode measured as a function of time when ignited. The infiltrated anodes were unreduced before test.

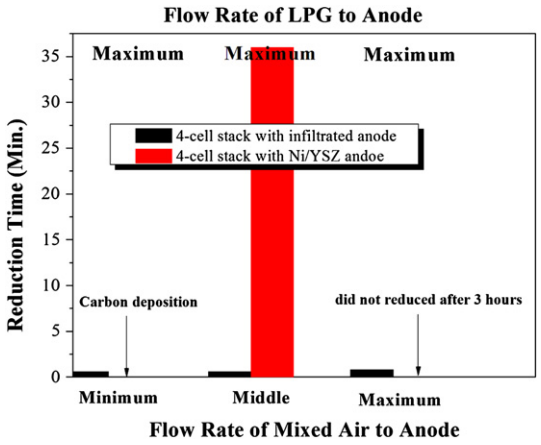

Fig. 7 – Start-up time for 4-cell stack with infiltrated anode or Ni/YSZ anode, under different test conditions. The flow rate of LPG was fixed to the maximum and the flow rate of mixed air was changed, in order to get different partial pressures of oxygen around anode. The flow rate of air to cathode was fixed at 200 sccm.

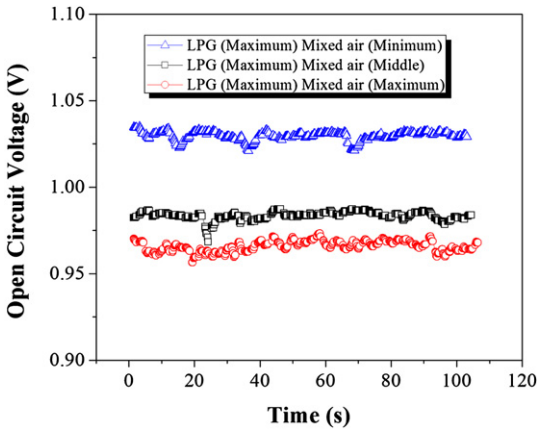

Fig. 8 – Average OCV values for 4-cell stack with infiltrated anode under different flow rates of mixed air to anode.

As for the conventional Ni/YSZ anode, the reduction time is about 36 min when the flow rates of LPG and mixed air to anode were adjusted to the states of maximum and middle, respectively. The time is much longer than that of perovskite based anode under the same test condition. It can be explained that NiO must suffer a volume loss of 41 vol.% for complete reduction to Ni catalyst, so much longer time should be required for the reduction/activation of Ni-based anodes [26,27]. But for the reduction/activation of perovskite-based anode, its activation just needs a decrease in valence state of metal ion (usually Cr and/or Mn) and an increase in oxygen vacancies, so quick-start will be available [28,33]. In this study, there was no time recorded for the reduction of Ni/YSZ anode at the states of (LPG Maximum, Mixed air Minimum) and (LPG Maximum, Mixed air Maximum). Because the reduced Ni was covered immediately with carbon soot under low oxygen content (LPG Maximum, Mixed air Minimum) and; at the same time, the LPG flow into anode was restricted by carbon soot, which must limit the further reduction of NiO inside anode. Under high oxygen content (LPG Maximum, Mixed air Maximum), the reduced Ni was oxidized immediately to NiO that could not be reduced completely, resulting in low OCV below 0.3 V during 3 h test of the 4-cell stack with Ni/YSZ anode.

3.4. *Initial fuel cell stack performance*

The OCV values of 4-cell stack with infiltrated anode at different oxygen contents, (LPG Maximum, Mixed air Minimum), (LPG Maximum, Mixed air Middle) and (LPG Maximum, Mixed air Maximum), were also given in Fig. 8. As expected, the maximum OCV value of 1.03 V (average value) appeared at the lowest oxygen content, corresponding to the state of (LPG Maximum, Mixed air Minimum). That is consistent with the theory value of Nernst equation [30]. When the flow rates of mixed air were adjusted to the states of middle and maximum, the OCV values were reduced to 0.98 V (average value) and 0.96 V (average value), respectively. During this test, only one variable is oxygen content. On the other hand, the variable is also the partial pressure of fuel around anode, which ultimately determines the cell OCV according to Nernst equation [31].

Fig. 9 shows some typical *I-V* characteristics for the 4-cell stack with infiltrated anode (with four cells connected in parallel) tested in an LPG flame (LPG Maximum, Mixed air Middle and air to cathode 200 sccm), demonstrating an OCV of 0.92 V and a peak power density of 348 mW cm^{-2} or a power of 223 mW, that is about 4 times higher than that of stack with its cathode operation outside flame [26]. It is noted that the stabilities in power output, OCV, and *I–V* curves for the cells operated inside flame (in this study) are much better than those for the cells with its cathode directly exposed to ambient air [24,26]. That should be attributed to the sealant-free configuration with an air manifold to cathode, which allows cells to operate inside flame, not only maintaining a stable operating temperature but also a reasonably stable and high partial pressure of oxygen at the cathode side. As for the 4-cell stack with the conventional Ni/YSZ anode, it exhibited an OCV of 0.915 V, slightly lower than that of perovskite based anode, and demonstrated a peak power density of 366 mW cm^{-2} or a power

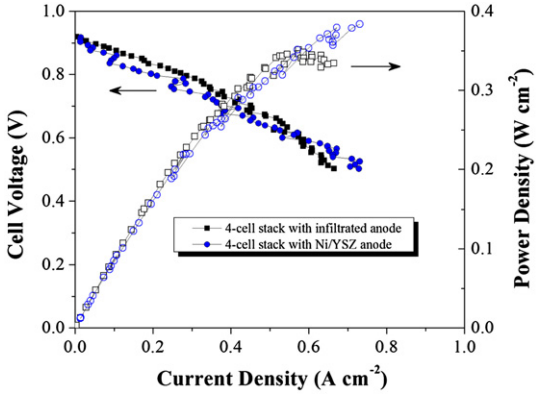

Fig. 9 – Cell voltage–current characteristics and power outputs of 4-cell stacks with different anodes operated inside LPG flame.

of 234 mW, slightly higher than that of infiltrated anode. It implies that the anode performance of the perovskite based anode can be compared with that of conventional Ni/YSZ anode. That should be attributed to the novel anode structure with a scaffold of yttria-stabilized zirconia (YSZ) infiltrated with a coating of LSCM and NiO. This design is to make effective use of the desirable properties of two different materials: the high oxygen ionic conductivity of an YSZ backbone and the excellent stability of LSCM coating. Moreover, the active sites of anode were also increased effectively by the application of infiltration technology. Furthermore, Ni as a catalyst also plays an important role on enhanced anode performance, which has been demonstrated in our previous work [33].

3.5. *Stability of the infiltrated anode and the system*

The stability of the cell depends critically on the stability of the anode, which may be deactivated by coking or contaminant poisoning in the flame of LPG. We used perovskite oxide LSCM as the primary phase of the infiltrated anode because it is reported to be an ideal replacement of the conventional Ni based anodes for operation in carbonaceous fuels, due to its good tolerance to carbon deposition and excellent redox stability at elevated temperatures [34,35]. Further, there was no sealant in the fuel cells, thus cell components may move freely to accommodate expansion and contraction associated with temperature fluctuation under the operating conditions. A 4-cell stack with infiltrated anode was operated for five thermal cycles (about 6 h for each) from 25 °C to about 850 °C at a fixed current of 0.45 A. The performance of the cell is shown in Fig. 10(a). After about 30 h of operation under the condition of (LPG Maximum, mixed air Middle and air to cathode 200 sccm), there was no obvious deterioration in cell performance, demonstrating not only redox stability and carbon resistance of the perovskite anode but also the thermal stability of the stack. But for Ni/YSZ anode, under the same test condition, the performance declined notably, 9% decrease after about 4 h test (2 redox-cycles). And, the start-up time for the 4-cell stack with Ni/YSZ anode was obviously longer than that of stack with infiltrated anode. It was about 40 min for the fist start-up, and about 30 min for the second start-up. For the infiltrated anode, the start-up times were all lower than 1 min for every redox-cycle.

Above experiment was conducted under the largest flow rate of LPG and a middle flow rate of mixed air to anode and 200 sccm flow rate of air to cathode. After the stability test, the cells anodes were all tested by a SEM to detect whether carbon deposition occurred during operation. There was no carbon

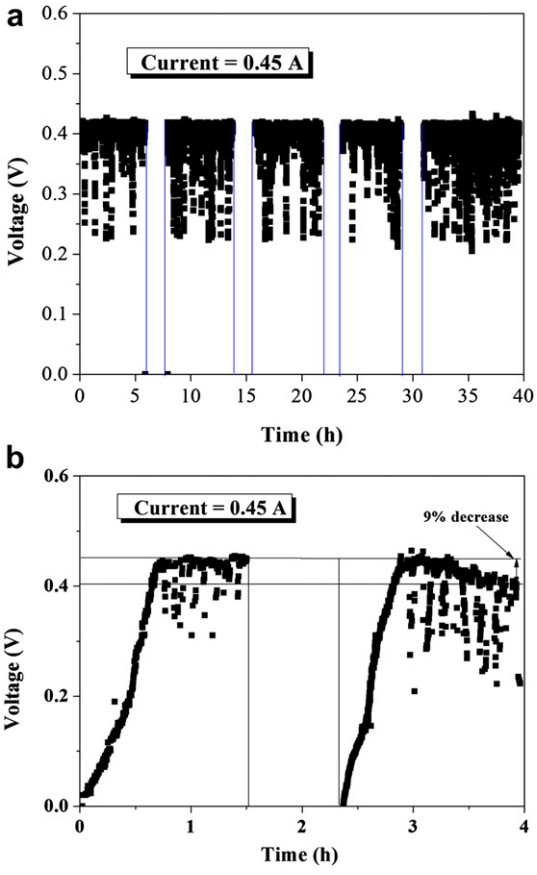

Fig. 10 – Cell voltage as a function of time for operation of the 4-cell stacks with (a) infiltrated anode and (b) Ni/YSZ anode at a total current of 0.45 A. The stack was operated for (a) five or (b) two thermal cycles from ~25 °C–~850 °C by placing (removing) the cell into (from) the flame directly.

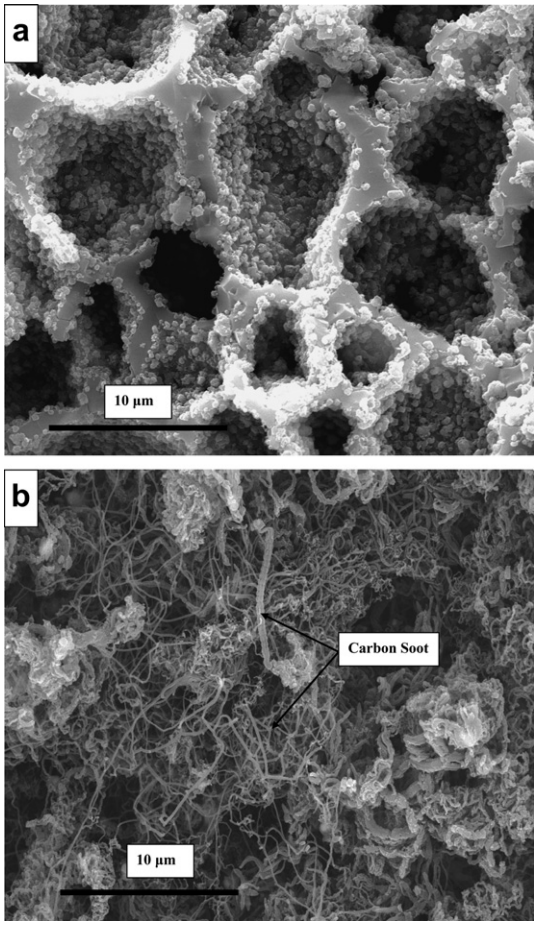

Fig. 11 – The carbon deposition of two kinds of anodes, (a) perovskite based (infiltrated) anode and (b) Ni/YSZ anode, after operation inside open LPG flame (almost pure LPG) for 1 h.

detected notably for the two anodes (infiltrated anode and Ni/YSZ anode), which may be caused by the relatively high oxygen content leading to the re-oxidation of carbon into CO_2 or CO. That also confirms that the Ni based anodes can be operated under these pre-mixed flames. In order to compare the carbon deposition on the two kinds of anodes, the flow rate of mixed air to anode was adjusted to minimum, i.e. almost pure LPG flow to anode. After about 1 h test, infiltrated anode was still in a good condition being like first, but for Ni/YSZ anode, two cells were broken by carbon deposition. That was also demonstrated by SEM images in Fig. 11. After the test, the inner surface of the infiltrated anode was still clean, free from carbon soot, whereas large amount of carbon soot were formed on the inner surface of the Ni/YSZ, demonstrating that the perovskite materials really have the ability for carbon resistance even when mixed with a small amount of Ni.

In this study, all cells were operated inside LPG flame that was heating water, indicating power can be produced during cooking and this CHP system was found to be practicable. DFFC can be successfully operated inside flame should be attributed to an air flow to cathode side. A CHP configuration with tubular SOFC without oxygen flow is under consideration in our group. The oxygen partial pressure near cathode will be maintained by the air convection.

4. Conclusions

A sealant-free micro-stack was successfully operated in a cooking system, demonstrating power can be produced with SOFC while cooking. Under the test conditions, a composite anode composed of a YSZ scaffold infiltrated with LSCM and NiO exhibited high performance, achieving a peak power density of 348 mW cm^{-2} without observable deterioration in performance after 5 thermal cycles with ~30 h of cumulative operation. This performance is 4 times higher than that of stack with the operation of cathode outside flame. And the performance of 348 mW cm^{-2} can be compared with 366 mW cm^{-2} of the stack with conventional Ni/YSZ anode. Besides that, this perovskite based anodes exhibited another two advantages: one is quick-start and the reduction/activation time is insensitive to partial pressure of oxygen; the other is it can be operated under a wide range of oxygen partial pressure. Under the same test conditions, the reduction/activation time for Ni/YSZ anode is 36 min, about 40 times of perovskite anode, and only operated under a small rang of oxygen partial pressure. After about 1 h test under diffusion flame of almost pure PLG, carbon deposition was not detected in the infiltrated anode but obvious for Ni/YSZ anode, suggesting that LSCM has good tolerance to carbon buildup and deactivation.

Acknowledgements

The authors thank the financial support from the Natural Science Foundation of China (20901020) and National High Technology Research Development Project of China (No. 2007AA05Z139).

REFERENCES

[1] Wu DW, Wang RZ. Combined cooling, heating and power: a review. Prog Energ Combust 2006;32:459–95.
[2] Packer J. Commercialisation of fuel cells for combined heat and power (CHP) application. J Power Sources 1992;37:101–9.
[3] Shabani B, Andrews J. An experimental investigation of a PEM fuel cell to supply both heat and power in a solar-hydrogen RAPS system. Int J Hydrogen Energy 2011;36:5442–52.
[4] Barelli L, Bidini G, Gallorini F, Ottaviano A. An energetice-exergetic comparison between PEMFC and SOFC-based micro-CHP systems. Int J Hydrogen Energy 2011;36:3206–14.
[5] Hawkes AD, Aguiar P, Hernandez-Aramburo CA, Leach MA, Brandon NP, Green TC, et al. Techno-economic modelling of a solid oxide fuel cell stack for micro combined heat and power. J Power Sources 2006;156:321–33.
[6] Kazempoor P, Dorer V, Weber A. Modelling and evaluation of building integrated SOFC systems. Int J Hydrogen Energy 2011;36:13241–9.
[7] Liso V, Olesen AC, Nielsen MP, Kær SK. Performance comparison between partial oxidation and methane steam reforming processes for solid oxide fuel cell (SOFC) micro combined heat and power (CHP) system. Energy 2011;36:4216–26.
[8] Farhad S, Hamdullahpur F, Yoo Y. Performance evaluation of different configurations of biogas-fuelled SOFC micro-CHP systems for residential applications. Int J Hydrogen Energy 2010;35:3758–68.
[9] Fontell E, Kivisaari T, Christiansen N, Hansen JB, Pålsson J. Conceptual study of a 250 kW planar SOFC system for CHP application. J Power Sources 2004;131:49–56.
[10] Nanaeda K, Mueller F, Brouwer J, Samuelsen S. Dynamic modeling and evaluation of solid oxide fuel cell – combined heat and power system operating strategies. J Power Sources 2010;195:3176–85.
[11] Braun RJ, Klein SA, Reindl DT. Evaluation of system configurations for solid oxide fuel cell-based micro-combined heat and power generators in residential applications. J Power Sources 2006;158:1290–305.
[12] Gorte RJ, Vohs JM. Nanostructured anodes for solid oxide fuel cells. Curr Opin Colloid Interface Sci 2009;14:236–44.
[13] Zhang XW, Chan SH, Li GJ, Hob HK, Li J, Feng ZP. A review of integration strategies for solid oxide fuel cells. J Power Sources 2010;195:685–702.
[14] Steele BCH, Heinzel A. Materials for fuel-cell technologies. Nature 2001;414:345–52.
[15] Atkinson A, Barnett SA, Gorte RJ, Irvine JTS, Mcevoy AJ, Mogensen M, et al. Advanced anodes for high temperature fuel cells. Nat Mater 2004;3:17–27.
[16] Riess I. On the single chamber solid oxide fuel cells. J Power Sources 2008;175:325–37.
[17] Yano M, Tomita A, Sano M, Hibino T. Recent advances in single-chamber solid oxide fuel cells: a review. Solid State Ionics 2007;177:3351–9.
[18] Shao ZP, Haile SM, Ahn J, Ronney PD, Zhan ZL, Barnett SA. A thermally self-sustained micro solid oxide fuel cell stack with high power density. Nature 2005;435:795–8.
[19] Hibino T, Wang SQ, Kakimoto S, Sano M. One-chamber solid oxide fuel cell constructed from a YSZ electrolyte with a Ni anode and LSM cathode. Solid State Ionics 2000;127:89–98.
[20] Horiuchi M, Suganuma S, Watanabe M. Electrochemical power generation directly from combustion flame of gases, liquids, and solids. J Electrochem Soc 2004;151(9):A1402–5.
[21] Horiuchi M, Katagiri F, Yoshiike J, Suganuma S, Tokutake Y, Kronemayer H, et al. Performance of a solid oxide fuel cell

couple operated via in situ catalytic partial oxidation of n-butane. J Power Sources 2009;189:950–7.
[22] Kronemayer H, Barzan D, Horiuchi M, Suganuma S, Tokutake Y, Schulz C, et al. A direct-flame solid oxide fuel cell (DFFC) operated on methane, propane, and butane. J Power Sources 2007;166:120–6.
[23] Wang K, Ran R, Hao Y, Shao ZP, Jin WQ, Xu NP. A high-performance no-chamber fuel cell operated on ethanol flame. J Power Sources 2008;177:33–9.
[24] Sun LL, Hao Y, Zhang CM, Ran R, Shao ZP. Coking-free direct-methanol-flame fuel cell with traditional nickel cermet anode. Int J Hydrogen Energy 2010;35:7971–81.
[25] Wang K, Zeng PY, Ahn JM. High performance direct flame fuel cell using a propane flame. P Combust Inst 2011;33:3431–7.
[26] Zhu XB, Lü Z, Wei B, Huang XQ, Wang ZH, Su WH. Direct flame SOFCs with $La_{0.75}Sr_{0.25}Cr_{0.5}Mn_{0.5}O_{3-\delta}$/Ni coimpregnated yttria-stabilized zirconia anodes operated on liquefied petroleum gas flame. J Electrochem Soc 2010;157(12):B2838–43.
[27] Zhu XB, Lü Z, Wei B, Zhang YH, Huang XQ, Su WH. Fabrication and evaluation of a Ni/$La_{0.75}Sr_{0.25}Cr_{0.5}Fe_{0.5}O_{3-\delta}$ co-impregnated yttria-stabilized zirconia anode for single-chamber solid oxide fuel cells. Int J Hydrogen Energy 2010;35:6897–904.
[28] Jardiel T, Caldes MT, Moser F, Hamon J, Gauthier G, Joubert O. New SOFC electrode materials: the Ni-substituted LSCM-based compounds $(La_{0.75}Sr_{0.25})(Cr_{0.5}Mn_{0.5-x}Ni_x)O_{3-\delta}$ and $(La_{0.75}Sr_{0.25})(Cr_{0.5-x}Ni_xMn_{0.5})O_{3-\delta}$. Solid State Ionics 2010;181:894–901.
[29] Zhu XB, Lü Z, Wei B, Liu ML, Huang XQ, Su WH. A comparison of $La_{0.75}Sr_{0.25}Cr_{0.5}Mn_{0.5}O_{3-\delta}$ and Ni impregnated porous YSZ anodes fabricated in two different ways for SOFCs. Electrochim Acta 2010;55:3932–8.
[30] Matsui T, Kosaka T, Inaba M, Mineshige A, Ogumi Z. Effects of mixed conduction on the open-circuit voltage of intermediate-temperature SOFCs based on Sm-doped ceria electrolytes. Solid State Ionics 2005;176:663–8.
[31] Nagel FP, Schildhauer TJ, Sfeir J, Schuler A, Biollaz SMA. The impact of sulfur on the performance of a solid oxide fuel cell (SOFC) system operated with hydrocarboneous fuel gas. J Power Sources 2009;189:1127–31.
[32] Zhu XB, Lü Z, Wei B, Zhang YH, Liu ML, Huang XQ, et al. Performance of the single-chamber solid oxide fuel cell with a $La_{0.75}Sr_{0.25}Cr_{0.5}Mn_{0.5}O_{3-\delta}$-based perovskite anode. J Electrochem Soc 2010;157(5):B691–6.
[33] Zhu XB, Lü Z, Wei B, Chen KF, Liu ML, Huang XQ, et al. Enhanced anode performance of solid oxide fuel cell with Ni/CeO_2 modified $La_{0.75}Sr_{0.25}Cr_{0.5}Mn_{0.5}O_{3-\delta}$ anode. J Power Sources 2009;190:326–30.
[34] Tao SW, Irvine JTS. A redox-stable efficient anode for solid oxide fuel cells. Nat Mater 2003;2:320–5.
[35] Fergus JW. Oxide anode materials for solid oxide fuel cells. Solid State Ionics 2006;177:1529–41.